Earth and Space Science

RESEARCH ARTICLE
10.1029/2018EA000468

An SOC Approach to Study the Solar Wind-Magnetosphere Energy Coupling

Adrija Banerjee[1], Amaresh Bej[1], T. N. Chatterjee[2], and Abhijit Majumdar[1]

[1]Department of Physics, Indian Institute of Engineering Science and Technology, Howrah, India, [2]Department of Electronics, Dinabandhu Andrews College, Kolkata, India

Key Points:
- The solar wind-magnetosphere coupling has been analyzed using a cellular automata model based on the concept of self-organized criticality
- A new coupling function is introduced to determine the cusp width
- A threshold value of B_Z, the zth component of the interplanetary magnetic field related to the yearly mean total number of sunspots, is introduced

Supporting Information:
- Supporting Information S1
- Data Set S1
- Data Set S2
- Data Set S3
- Data Set S4

Correspondence to:
A. Bej,
amaresh_bej@yahoo.com

Citation:
Banerjee, A., Bej, A., Chatterjee, T. N., & Majumdar, A. (2019). An SOC approach to study the solar wind-magnetosphere energy coupling. *Earth and Space Science*, *6*, 565–576. https://doi.org/10.1029/2018EA000468

Received 5 SEP 2018
Accepted 3 FEB 2019
Accepted article online 6 FEB 2019
Published online 8 APR 2019

Abstract Solar wind-magnetosphere interaction and the injection of large quantity of plasma particles into the Earth's magnetosphere are the primary reasons behind geomagnetic storm, auroral effects, and, in general, all the fluctuations observed in the terrestrial magnetic field. In this paper, we analyzed the perturbed magnetosphere as a sandpile-like cellular automata model based on the concept of self-organized criticality and many-body interactive system and proposed a solar wind-magnetosphere energy coupling function in terms of interplanetary magnetic field B_Z, the zth component of interplanetary magnetic field. The function determines the cusp width W depending on the intensity of $(-B_Z - B_{\mathrm{Th}})$ where B_{Th} is the threshold value. The model generates two output series, which are the numerical representation of the real-time *Dst* index and *AE* index series, respectively. For our study, the range of years 1997–2007 of the 23rd solar cycle had been considered here. The threshold value B_{Th} plays a significant role in the analysis and exhibits a proportional relationship with the yearly mean total number of sunspots for each year of the range 1997–2007 of the 23rd solar cycle. For each year, the two resultant output time series of the model display high-correlation coefficients with the real-time *Dst* and *AE* indexes, respectively, which denotes the acceptability of the proposed energy coupling function and its relation with the solar activities.

1. Introduction

The solar wind-magnetosphere interaction and the energy coupling can be considered as the key factor to understand the various dynamical properties of the terrestrial magnetosphere. The solar wind, a stream of highly energized plasma particles, emitted from the Sun's outer atmosphere, is coming toward the Earth with an average speed of 400 km/s. These huge amounts of particles are injected into the Earth's magnetosphere through the cusps controlled by the zth component of the interplanetary magnetic field (IMF), B_Z. The direction and magnitude of IMF B_Z is the primary controller of the solar wind-magnetosphere reconnection along with the dynamic pressure of the solar wind. A detailed knowledge of the energy coupling mechanism is important to estimate the total amount of injected solar wind energy in the geospace as this energy drives all the geomagnetic fluctuations in the terrestrial magnetosphere, causing intense geomagnetic storm or auroral activities (Russell, 2000, 2013).

Extreme geomagnetic activity is considered to be a serious threat to the Earth's technological and electrical systems. In the time of severe geomagnetic storm, solar wind injects a large amount of ionized particles into the Earth's magnetosphere, rapidly changing the intensity of the magnetic field which in turn induces an electric field on the surface of the Earth. This induced electric field then drives a current through any electrical network by forming a potential difference between the ground points of that network. This current is known as geomagnetically induced current (GIC). The intensity of GIC has been noted as large as over 100 A, though a few amperes is sufficient to unexpectedly collapse any electrical infrastructure causing a huge loss of money and related hazards (Kappenman et al., 1997). The 13 March 1989 geomagnetic storm and the complete collapse of Hydro Quebec power grid resulting in 9 hr blackout for 6 million customers [Hydro-Québec, Understanding Electricity,1989; Kappenman et al., 1997], the 30-hr blackout of the Wide Area Augmentation System managed by the Federal Aviation Administration, and the damage of Japanese ADEOS-2 satellite due to the Halloween solar storm in 2003 are some of the most prominent examples [CENTRA Technology Inc. report 2011; NOAA Technical Memorandum 2003; Workshop report of National Research Council of the National Academics 2008]. Also, past records of GIC-triggered hazards include complete disruption of power grids and transformers; malfunction of railway equipment and satellite hardware; severe collapsing of telecommunication, navigation, and computer systems; and increase of

steel corrosion in pipeline networks, particularly in countries like the United States and Canada or northern Europe, located in the upper latitudes and affected most by the auroral electrojet current [CENTRA Technology Inc. report 2011; Kappenman et al., 1997; NOAA Technical Memorandum 2003]. So a comprehensive knowledge of the solar wind-magnetosphere interaction and the underlying physical process of geomagnetic activity is crucial to save human society from its severe negative effects.

The solar wind-magnetosphere energy coupling mechanism became a subject of keen interest and curiosity in the past decades. The complex dynamics of the energy coupling process, the rate of energy transfer into the magnetosphere, and the distribution of the injected energy in the magnetosphere-ionosphere system as well as the role of the various solar wind parameters controlling the overall process had been rigorously studied, analyzed, and characterized in numerous works. A number of solar wind energy coupling functions had been presented (Akasofu, 1981; Finch & Lockwood, 2007; Gonzalez, 1990; Gonzalez et al., 1989; Kan & Lee, 1979; Newell et al., 2007; Perreault & Akasofu, 1978), while the nature of solar wind-magnetosphere interaction had been extensively studied in relation with the other solar wind parameters like velocity, ion density, and dynamic pressure [Crooker et al., 1977; Crooker & Gringauz, 1993; Dungey, 1961; Mawad et al., 2016; Newell et al., 2007; Papitashvili et al., 2000; Temerin & Li, 2006; Wygant et al., 1983; Youssef et al., 2011]. Global magnetohydrodynamic simulations [Palmroth et al., 2003, 2005, 2006, 2010, 2012; Papadopoulos et al., 1999. Pulkkinen et al., 2002, 2008, 2010; Wang et al., 2014] along with various other methods (Bargatze et al., 1986; Murayama, 1982; Stamper et al., 1999) were also taken into account. The estimation of the percentage of solar wind energy injected into the geospace, how much of this energy is dissipating in the magnetosphere or in the ionosphere, and in general the entire energy transfer and dissipation process long became the focus point of detailed investigations [Lu et al., 1998, 2013; Scurry & Russell, 1991; Stern, 1984; Tanskanen et al., 2002; Tenfjord & Ostgaard, 2013; Turner et al., 2001; Østgaard et al., 2002; Vasyliunas et al., 1982]. Though all these serious efforts produced significant results, solar wind-magnetosphere-ionosphere interaction still demands further attention to understand the complex nature of geomagnetic disturbances.

In our previous work, we came to realize that geomagnetic disturbances on the Earth is an essentially complex natural phenomenon having a number of underlying dynamics and quite impossible to predict accurately, whereas *Dst* index, the measurement of geomagnetic activity, is a positively correlated fractional Brownian motion having long-range correlation (Banerjee et al., 2011). Enlightened by this outcome, we aimed to develop a sandpile-like cellular automata model, analogous to the Earth's magnetosphere to investigate the dynamical characteristics of the geomagnetic storm (Banerjee et al., 2015). Now sandpile model was selected as the first example displaying the concept of self-organized criticality, introduced by Bak et al. in their 1987, 1988 pioneering papers. Since then, this algorithm had been extensively used to study and analysis the physical process of geomagnetic fluctuations (Chang, 1992, 1999; Chapman et al., 1998; Consolini, 1997; Consolini & Lui, 1999; Klimas et al., 2000; Takalo et al., 1999; Uritsky, 1996; Uritsky & Pudovkin, 1998a, 1998b; Uritsky & Semenov, 2000). Our proposed 2015 model was a dissipative dynamical system with both spatial and temporal degrees of freedom, based on the concept of self-organized criticality and a refined version of the model presented by Uritsky et al. (2001). Though it was a first-order model with basic considerations, the resultant time series exhibited similar statistical characteristics of the real-time *Dst* index. The acceptability of the model and its curious outcome made us realize the significance of the solar wind-magnetosphere interaction and motivated us to further investigate the true nature of the energy coupling mechanism.

In the present paper, we continued our analysis based on the sandpile-like cellular automata model of the terrestrial magnetosphere, presented in our 2015 paper (Banerjee et al., 2015). We proposed a definite solar wind-magnetosphere energy coupling function in terms of IMF B_Z and a threshold value, B_{Th}. The function is a hyperbolic tangent one which determines the cusp width W at any time t. The model produces two output series which are the numerical representations of the real-time *Dst* index and *AE* index series, respectively. To examine the validity of the proposed energy coupling function, the correlation coefficients between the simulated output series, the real-time *Dst*, and *AE* index series had been estimated respectively. The entire 23rd solar cycle had been studied, and the real-time data of solar ion density, flow speed, and IMF B_Z had been considered here. The result shows significant values of correlation coefficients between the simulated and real-time series for a specific value of the B_{Th} for each year. The parameter B_{Th} plays a key

role here as it varies exactly proportionally to the variation of the yearly mean total number of sunspots for each year of the range 1997–2007 of the 23rd solar cycle, revealing the direct influence of solar activities on the solar wind-magnetosphere reconnection phenomena.

2. Method

The cellular automata-based sandpile model presented here is a refinement of the model proposed in our previous paper (Banerjee et al., 2015). In summary, the model, a numerical representation of the Earth's magnetosphere, is a finite matrix of $n \times n$ elements, characterized by energy E, which is a function of time and space. With analogy to the Earth, open boundary condition had been considered, denoting upper ($i = 1$, $j = 1$ to n) and lower ($i = n, j = 1$ to n) boundary regions of the system. Solar wind emitted from the Sun is coming toward the Earth. It interacts with the terrestrial magnetosphere, a reconnection occurs, and a significant amount of ionized particle penetrates into the geospace through the cusp, altering its energy. The energy unit dE at any time t is calculated using the real-time ion density and flow speed data obeying the equation

$$\mathrm{d}E(t) = \mathrm{norm}\left({}^{1}/_{2}\times\text{ion density}\times(\text{flow speed})^{2}\right) \tag{1}$$

For initialization, each of the cells of the matrix is credited with a small amount of solar wind energy following the equations

$$E_{t+1}(i,j) = E_{t}(i,j) + K_{r}\times\mathrm{d}E(t) \text{ for } i = 2 \text{ to } n+1, j = 1 \text{ to } n \tag{2}$$

and

$$E_{t+1}(i,j) = E_{t}(i,j) + K_{a}\times\mathrm{d}E(t) \text{ for } i = 1, j = 1 \text{ to } n \tag{3}$$

where K_{r} and K_{a} are constants.

Both the direction and the intensity of the zth component of the IMF, B_Z determines the cusp width W, thus controlling the amount of energy injected into the system. For the cellular automata model of $n \times n$ matrix presented here, the cusp width W is a square of cells surrounding the cell ($i = n/2, j = n/2$), that is, the cell in the center of the matrix. For a large northward B_Z, the cusp width W is minimum 0, whereas for a large southward B_Z, the cusp width W has a maximum value, $W_{m} = (n-1)^2$. W_{m} has a constant value for a constant n.

The functional relationship of W and B_Z proposed here is

$$W(t) = W_{m}{}^{*}\left((\tanh((-B_Z - B_{Th})/\lambda)) + 1\right)/2 \tag{4}$$

where B_{Th} is the threshold value of IMF B_Z to open up the cusp and λ is a constant. The parameter B_{Th} is the most significant factor in the entire analysis as it controls the net amount of solar wind-magnetosphere energy coupling area. At any time t, the hyperbolic tangent term in equation (4) generates a value in the range of 0 to 1. For a large southward B_Z, the hyperbolic tangent term is 1 and $W = W_{m}$, whereas for a large northward B_Z the term is 0 and $W = 0$. In between the extrema, W has an intermediate value depending on the value of $(-B_Z - B_{Th})$. W has a numeric value.

The input energy d$E(t)$ is injected into the model through W number of cells following the equation

$$E_{t+1}(i,j) = E_{t}(i,j) + \mathrm{d}E(t) \text{ for } i = n/2\pm p, j = n/2\pm p \tag{5}$$

where $p = \mathrm{round}\left((\sqrt{W} - 1)/2\right)$.

Now if the altered energy of the cell (i,j) crosses the threshold value E_{Th} of the system, the excess energy is distributed among the adjacent neighbors obeying the equations

$$E_{t+1}(i,j) = E_t(i,j) - 4 \tag{6}$$

and

$$E_{t+1}(i \pm 1, j \pm 1) = E_t(i \pm 1, j \pm 1) + (1 - E_d/4) \tag{7}$$

where E_d is the dissipation factor and $(i \pm 1) \geq 1$ or 2 according to the case.

The total energy of the system at any time t can be calculated as

$$E_1(t) = \Sigma E(i,j) \text{ for } i = 2 \text{ to } n+1, j = 1 \text{ to } n \tag{8}$$

The differential value of the energy stored in the system at any time t is then estimated by

$$E_2(t) = \Delta E_1(t) \tag{9}$$

For further refinement, the above time series is then processed by a moving-average filter of span 72 to get the final output series as

$$E_r(t) = -\mathrm{MA}(E_2) \tag{10}$$

$E_r(t)$ is an estimation of the differential value of the energy stored in the system and can be considered as a numerical equivalent to the *Dst* index. Now a high correlation coefficient between the simulated series $E_r(t)$ and the real-time *Dst* index can establish the validity of the proposed coupling function.

The real-time hourly averaged *Dst* index data set has been obtained from OMNIWeb. To remove the noise and fine-scale structure, the data set is further processed by a moving-average filter of span 72 to get a series, namely, $E_{Dst}(t + T)$ where T denotes the time shift or time lag. Now cross correlation is considered as a standard technique to measure the degree of similarity between two time series, and this method had been applied here to determine the correlation between the series $E_r(t)$ and $E_{Dst}(t + T)$. To estimate the optimum cross-correlation coefficient between these two series, the series $E_r(t)$ had been compared to the time-shifted real-time *Dst* index, $E_{Dst}(t + T)$ where T is varied in the range of values 0 to 720 hr, and for each value of T, the correlation coefficients between the two series had been noted down along with the exact value of T. Here T is the lag value of duration 1 hr associated with the cross-correlation method.

As open boundary condition has been considered, the excess energy transmits outside the grid after reaching the upper ($i = 1, j = 1$ to n) and lower ($i = n + 2, j = 1$ to n) boundary regions of the system. With analogy to the Earth, these upper and lower boundaries can be considered as the northern and southern polar cusps of the Earth, while this energy transfer process is similar to the transmission of the excess energy of the Earth's magnetosphere to the ionosphere through the polar cusps. Thus, the amount of excess energy dissipated through the upper boundary or northern polar cusp can be estimated as

$$E_3(t) = \Sigma E(i,j) \text{ for } i = 1, j = 1 \text{ to } n \tag{11}$$

and the differential energy value as

$$E_4(t) = \Delta E_3(t) \tag{12}$$

Similarly, as equation (10) the moving-average technique has been applied to equation (12) to get the following one

$$E_a(t) = \mathrm{MA}(E_4) \tag{13}$$

Equation (13) is the measurement of the excess energy dissipated in the ionosphere from the magnetosphere through the polar cusps and can be considered as a numerical representation of the auroral electrojet (*AE*) index. Similar as before, the real-time *AE* index data series has been obtained from OMNIWeb and further processed by a moving-average filter of span 72 to get the series $E_{AE}(t + T)$, where T is the time shift or time lag. Again, the method of cross correlation had been applied here to determine the amount of correlation

between the two series $E_a(t)$ and $E_{AE}(t+T)$, considering T as the associated lag value of duration 1 hr. The correlation coefficients between the simulated series $E_a(t)$ of equation (13) and the real-time $E_{AE}(t+T)$ had been estimated to further strengthen the validity of the proposed coupling function. Here also, the series $E_a(t)$ had been compared with the time-shifted *AE* index, $E_{AE}(t+T)$ where T is varied in the range of values 0 to 720 hr to achieve the optimum correlation coefficient between the two series. For each value of T, the associated correlation coefficients had been recorded.

As mentioned before, the threshold value B_{Th} of equation (4) is playing the key role in the entire analysis as the term $(-B_Z - B_{Th})$ controls the widening or narrowing of the cusp width and the amount of solar wind energy injected into the magnetosphere at any time t. In this work, we had studied the variation of the magnitude of the solar wind-magnetosphere coupling with variation of B_{Th} and its subsequent effect on the overall dynamics of the system.

3. Data source

Here we used the hourly averaged *Dst* index, *AE* index, solar wind ion density, flow speed, and B_Z component of the IMF data from the year 1997 to the year 2007 as extracted from NASA/GSFC's (Goddard Space Flight Center) OMNI data set through OMNIWeb (King & Papitashvili, 2005). The OMNI data were obtained from the GSFC/SPDF (Space Physics Data Facility) OMNIWeb interface at the OMNIWeb website (http://omniweb.gsfc.nasa.gov). We used the *Dst* index and *AE* index data obtained from OMNIWeb to compare with the estimated series $E_r(t)$ and $E_a(t)$, respectively.

For the yearly mean total number of sunspots, the source credit is the sunspot data from the World Data Center SILSO (Sunspot Index and Long-term Solar Observations; Sunspot Number and Long-term Solar Observations, Royal Observatory of Belgium, on-line Sunspot Number catalogue: http://www.sidc.be/SILSO/, '1997–2007').

4. Result and Discussions

To study the dynamics of the system depending on the solar wind-magnetosphere coupling, we had considered the range of years 1997 to 2007 of the 23rd solar cycle. The input energy dE had been calculated using equation (1) and using the real-time value of flow speed and ion density. The cellular automata model is a matrix having a dimension of $n \times n$. Here it is taken as $n = 50$, that is, the matrix contains 50×50 cells. The input energy dE(t), calculated from OMNIWeb data is an one-dimensional time series. At any time t, the total cusp area W is determined using equation (4). The cusp area is a square having the cells $i = 25 \pm p, j = 25 \pm p$ where p = round $((\sqrt{W} - 1)/2)$. The input energy d$E(t)$ is injected into all these cells of $i = 25 \pm p, j = 25 \pm p$ according to equation (5) stated in the section 2. The values of the different parameters are taken as $E_{Th} = 5$, $E_d = 0.001$, $K_r = 0.001$, $K_a = 0.1$, $\lambda = 0.5$. All these values are constants for each of the year in the range of 1997–2007. As referred in the section 2, our sandpile model is a refined version of the model presented in our 2015 paper which was based on the model proposed by Uritsky et al. (2001). Uritsky et al. set the threshold of excitation as $E_{Th} = 5$ and suggested the value of the dissipation term $E_d <= 0.01$ to study the wide-range scale-invariant behavior of the system. Following their work, we also set $E_{Th} = 5$ and $E_d = 0.001$ for our model. We studied the model for different values of K_r, K_a, and λ and observed that the model output series matches best with the real-time series for values $K_r = 0.001$, $K_a = 0.1$, and $\lambda = 0.5$. So we considered these values of K_r, K_a, and λ constants for our entire analysis.

For each year, the value of parameter B_{Th} had been varied in the range of −10.00 to 10.00 nT, and for each value of B_{Th} within this range, the correlation coefficients between the simulated series $E_r(t)$ of equation (10) and the time-shifted real-time *Dst* index series $E_{Dst}(t+T)$ as well as the series $E_a(t)$ of equation (13) and the time-shifted real-time *AE* index series $E_{AE}(t+T)$ had been estimated respectively. While calculating the correlation coefficients for the above two cases, the value of time lag T had been varied from $T = 0$ to 720 hr to achieve the optimum value of the coefficients. Thus, the best correlation coefficient for each set is found annually. The exact value of B_{Th} and the particular value of T associated with the optimum coefficients had been noted down along with the value of the coefficients. Table 1 displays the optimum values of the correlation coefficients for each year in the range of 1997 to 2007 with the corresponding values of the

Table 1
The First Three Columns of the Table Shows the Yearly Mean Total Number of Sunspots and the Values of the Threshold B_Z, B_{Th} for All the Years in the Range of 1997–2007

			Comparison between $E_r(t)$ and $E_{Dst}(t+T)$		Comparison between $E_a(t)$ and $E_{AE}(t+T)$	
Year	Yearly mean total number of sunspots	B_{Th} (nT)	Optimum correlation coefficient (%)	Time lag T (hr)	Optimum correlation coefficient (%)	Time lag T (hr)
1997	28.90	1.25	70.27	24	74.53	2
1998	88.30	1.76	60.47	32	77.05	4
1999	136.30	2.18	64.23	24	66.06	5
2000	173.90	2.50	76.06	25	69.02	2
2001	170.40	2.47	72.64	21	72.28	0
2002	163.60	2.41	75.83	31	75.42	8
2003	99.30	1.86	62.99	25	59.47	10
2004	65.30	1.56	75.26	16	76.37	3
2005	45.80	1.40	60.64	35	75.96	11
2006	24.70	1.21	52.83	30	74.63	6
2007	12.60	1.10	62.79	43	81.18	12

Note. For this entire range of years, the optimum correlation coefficients between the simulated series $E_r(t)$ and the time-shifted real-time *Dst* index series $E_{Dst}(t+T)$ and the associated values of time lag T are displayed in the fourth and fifth columns, respectively, while in a similar fashion, the sixth and seventh columns show the optimum correlation coefficients between the simulated series $E_a(t)$ and the time-shifted real-time *AE* index series $E_{AE}(t+T)$ and the corresponding values of time lag T, respectively.

parameter B_{Th} and also the values of T for both the cases. The correlation coefficient R between two series A and B is calculated using the equation

$$R = \frac{\sum_m \sum_n (A_{mn} - \overline{A})(B_{mn} - \overline{B})}{\sqrt{\left(\sum_m \sum_n (A_{mn} - \overline{A})\right)^2 \left(\sum_m \sum_n (B_{mn} - \overline{B})\right)^2}} \quad (14)$$

Figure 1 represents a comparison between the actual waveforms of the simulated series $E_r(t)$ and the real-time *Dst* index series $E_{Dst}(t+T)$ where $T = 31$ for the year of 2002. The optimum correlation coefficient between these two series is 75.83% for $B_{Th} = 2.41$ and $T = 31$ in this year. The top half of Figure 1 shows the waveform of simulated output series $E_r(t)$, while the bottom half shows the waveform of the time-shifted *Dst* index series, $E_{Dst}(t+T)$ for the year 2002. Both the series are 1-hourly time series having 8,578 data each. The time in hour is plotted in the x axis. Here 8,000 means $t = 8{,}000$, that is, the point of 8,000th hour. Each of the year in the range of 1997–2007 contains 8,000–9,000 data.

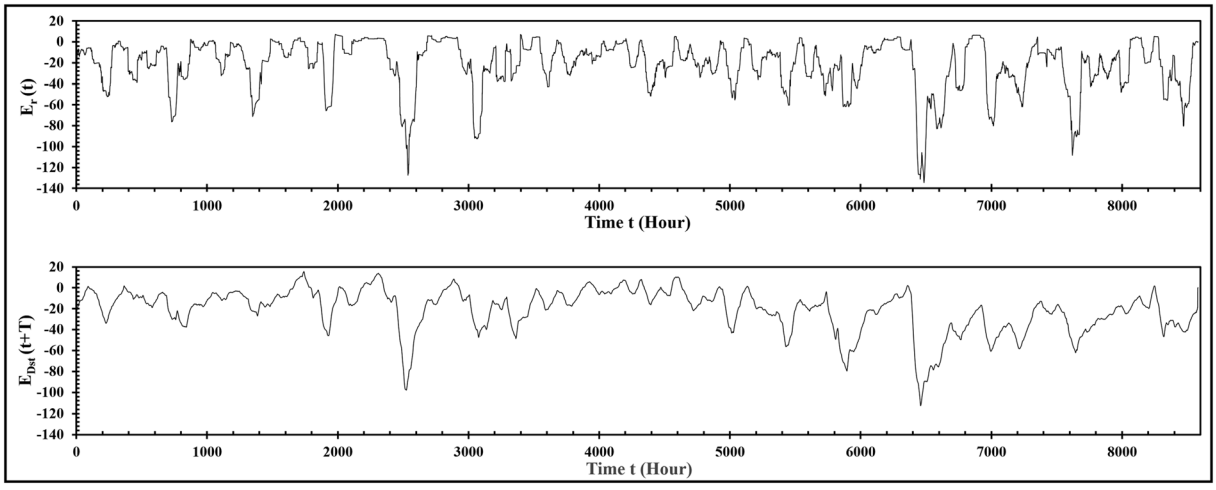

Figure 1. (top) The plot of simulated output series $E_r(t)$ and (bottom) the plot of the time-shifted *Dst* index series, $E_{Dst}(t+T)$ where $T = 31$ for the year 2002. Both the series are plotted with respect to time (hours). The value of $B_{Th} = 2.41$ for this year and the optimum correlation coefficient between the two series is 75.83%. The correlation coefficient between the two series is estimated using equation (14).

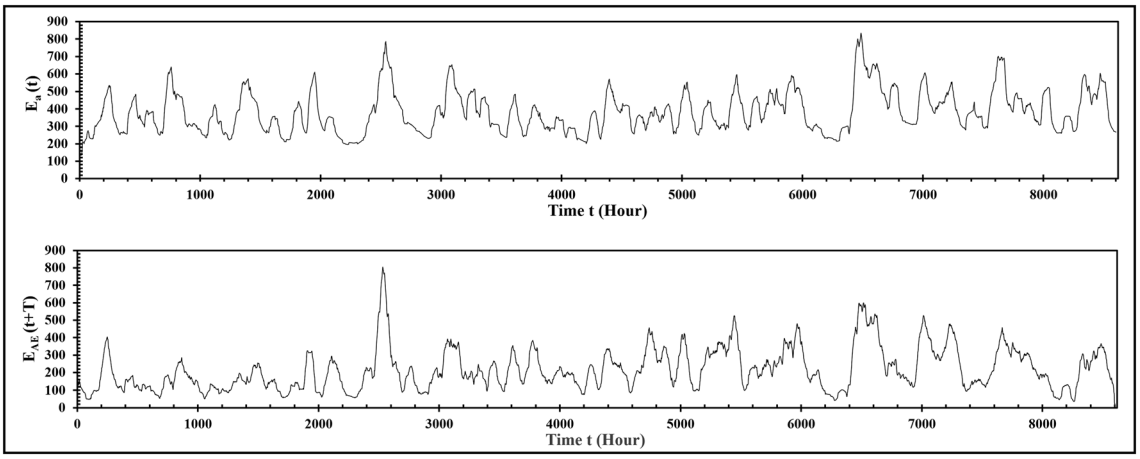

Figure 2. (top) The plot of simulated output series $E_a(t)$ and (bottom) the plot of the time-shifted *AE* index series, $E_{AE}(t + T)$ where $T = 8$ for the year 2002. Both the series are plotted with respect to time (hours). The value of $B_{Th} = 2.41$ for this year and the optimum correlation coefficient between the two series is 75.42%. The correlation coefficient between the two series is estimated using equation (14).

Figure 2 displays the graphs of the simulated series $E_a(t)$ and the real-time *AE* index $E_{AE}(t + T)$ where $T = 8$, also for the year of 2002. Here the optimum correlation coefficient between these two series is 75.42% for $B_{Th} = 2.41$ and $T = 8$. The top half of Figure 2 shows the waveform of simulated output series $E_a(t)$, while the bottom half shows the waveform of the time-shifted *AE* index series, $E_{AE}(t + T)$ for the year 2002. Both the series are 1-hourly time series having 8,601 data each. The time in hour is plotted in the *x* axis.

The current work is focused to propose a solar wind-magnetosphere energy coupling function and to study the subsequent energy transfer process using a cellular automata model of Earth's magnetosphere. To establish the validity of the model and the coupling function, the model had been simulated numerously for different set of values of the controlling parameters. For every simulation, the model output series had been compared with the real-time series. Finally, it is observed that for the set of values $K_r = 0.001$, $K_a = 0.1$, and $\lambda = 0.5$ the model output series matches best with the real-time series. So we have considered these set of values constant for the entire range of the years 1997–2007. Now T denotes the time gap between the injection of the plasma particles into the magnetosphere and its subsequent effect on the intensity of the horizontal magnetic field of the Earth. As the amount of injected energy into the magnetosphere is not same for every year, the value of T cannot be assumed as a constant for every year beforehand; rather its value for each year had been obtained from the result.

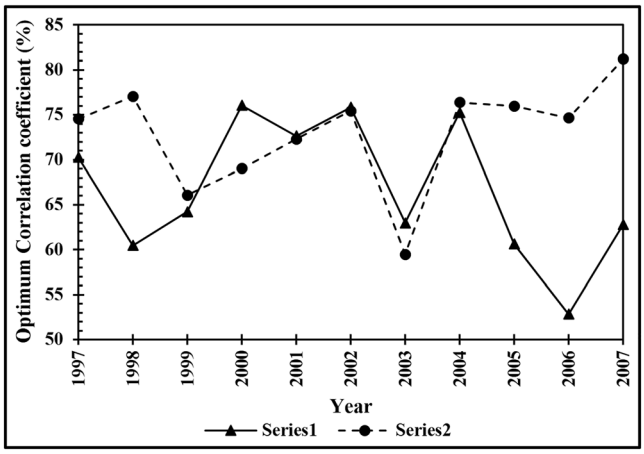

Figure 3. Series 1 is the yearly plot of the optimum correlation coefficients between the simulated series $E_r(t)$ and the time-shifted real-time *Dst* index series $E_{Dst}(t + T)$. Series 2 is the yearly plot of the optimum correlation coefficients between the simulated series $E_a(t)$ and the time-shifted real-time *AE* index series $E_{AE}(t + T)$. Year, in the range of 1997–2007 is plotted in the *x* axis.

Figure 3 shows the plot of optimum correlation coefficient for each of the years in the range of 1997–2007 for both sets of data, as obtained from Table 1.

The above result exhibits a striking connection of the solar wind-magnetosphere reconnection with solar activities. Table 1 also shows the yearly mean total number of sunspots for each year in the range of 1997–2007 of the 23rd solar cycle. As shown in Figure 4, for the entire range of years, the parameter B_{Th} varies proportionally with the yearly mean total number of sunspots. The value of B_{Th} is maximum 2.5 in the year 2000 which is also the year of solar maxima having 173.9 yearly mean total number of sunspots, while B_{Th} reaches its minimum value 1.1 in the year where the yearly mean total number of sunspots is only 12.6.

Studying the above observations thoroughly, we came to realize some significant and meaningful points about the solar wind-magnetosphere coupling and the resultant geomagnetic disturbances which can be discussed

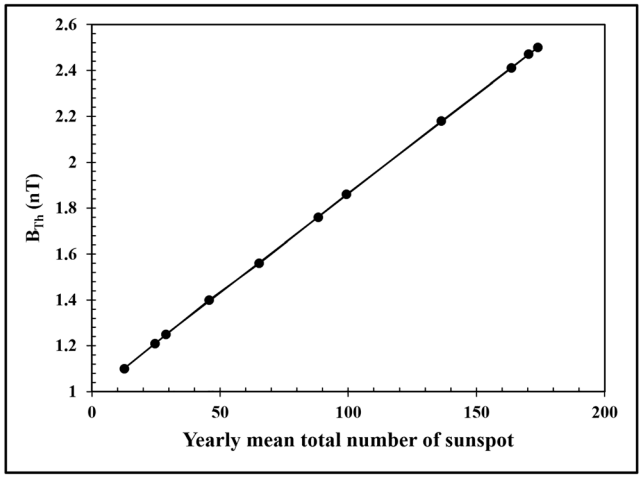

Figure 4. The threshold value, B_{Th}, is plotted with respect to the yearly mean total number of sunspots for the range of years 1997–2007 of the 23rd solar cycle. The graph shows a proportional relationship between these two parameters.

here now. First of all, the cusp width W due to the magnetic reconnection is not a linear function of IMF B_Z but a hyperbolic tangent one which takes into account both the direction and magnitude of IMF B_Z and also the threshold value, B_{Th}. For large northward B_Z, the value of the function is close to 0, and the cusp is almost closed; the amount of injected particles into the magnetosphere is negligible. As the magnitude of the northward B_Z reduces below the threshold value, B_{Th}, the cusp width W starts to widen out resulting in a substantial amount of injection into the magnetosphere. As the IMF B_Z changes direction and becomes southward, the cusp width widens out further and continues to do so as long as the magnitude of the southward B_Z increases. The amount of injected particles into the magnetosphere increases rapidly with the increasing cusp width. Numerically, the cusp width can be a minimum zero value or completely closed for an extreme northward B_Z or can obtain a maximum value or completely open for an extreme southward B_Z. Between these extrema, it varies proportionally with the variation of the magnitude of $(-B_Z - B_{Th})$.

Second, the correlation coefficients between the simulated and output series, shown in Table 1, exhibit moderate to high values and support the rightness of the proposed coupling function in two ways, first in connection with the stored energy in the magnetosphere and *Dst* index and second in connection with the excess energy dissipated into the ionosphere and *AE* index. The correlation coefficients are associated to a particular value of the parameter B_{Th} for each year. Most significantly, the parameter B_{Th} displays a proportional relationship with the yearly mean total number of sunspots for the entire solar cycle, revealing an influence of solar activities on the threshold value, B_{Th}. Higher number of solar spots indicates higher solar activity which increases solar wind and also the coronal mass ejections, resulting in an injection of huge amount of plasma particles into the terrestrial magnetosphere. The magnetic fields associated with coronal mass ejections also play a significant role in magnetic reconnection. In this case, the cusp opens up for a comparatively higher value of northward B_Z. Now the threshold value of B_Z to open up the cusp and enable the energy injection process into the magnetosphere is denoted by B_{Th}, and it is observed from the result that the value of B_{Th} is the highest at 2.5 nT of northward B_Z in the year 2000, the year of solar maxima of the 23rd cycle having 119.6 number of solar spots. On the other hand, a lower value of B_{Th} is observed in the years with lower number of solar spots. The year 2007 observed only 7.6 number of sun spots and the threshold value of B_{Th} is 1.1 nT of northward B_Z for that particular year.

Finally, some meaningful insights can be extracted from the number of shifts associated with the value of the correlation coefficients for both sets of data series for each year. To estimate the optimum value of correlation between the simulated series and the real-time series, the simulated series had been compared to the real-time series shifted by T hours. The value of T is different for different years. For the year 2002, the optimum correlation coefficient between the simulated series $E_r(t)$ and $E_{Dst}(t + T)$ is 75.83% where $T = 31$. The injected plasma particles into the terrestrial magnetosphere generates the ring current which in turn deviates the intensity of the Earth's horizontal magnetic field from its average value. This deviation is measured and termed as *Dst* index. Here in this work, the output time series $E_r(t)$ is an estimation of the total amount of energy in the system after injection and its subsequent distribution of the input energy at any time t, and it is considered a simulated representation of this solar wind energy trapped in the magnetosphere responsible for generating the *Dst* index. The observation that the series $E_r(t)$ matches best with the real-time series $E_{Dst}(t + T)$ where $T = 31$ for the year of 2002 implies that the injected input energy at any time t affects the Earth's horizontal magnetic field at $(t + 31)$ hours in that very year. Similarly as the year 2002, such a time interval of 16–43 hr between the energy injection into the magnetosphere and the effective depression of horizontal magnetic field from its average value is present for all the years of the range 1997 to 2007 of the 23rd solar cycle as can be seen from Table 1.

The same observation had been noted down in the case of estimating the correlation between the simulated series $E_a(t)$ and the real-time *AE* index, $E_{AE}(t + T)$ also. The extra solar wind energy injected into the

magnetosphere is released into the ionosphere generating the westward and eastward electrojet currents in the auroral regions. *AE* index is calculated as the average value of *AU* and *AL* indexes, which in turn are the measurements of the highest and lowest depressions of the auroral magnetic field from its average value due to these westward and eastward electrojet currents, respectively. In our model the simulated output series $E_a(t)$ is equivalent to the excess energy released into the ionosphere, responsible for forming the *AE* index. For the year of 2002, the optimum value of correlation coefficient between the two series is $E_a(t)$, and $E_{AE}(t+T)$ is 75.42% for $T = 8$, which denotes a time interval of 8 hr between the energy release into the ionosphere and the depression of auroral magnetic field. All the years of 23rd solar cycle exhibit a time interval of 0 to 12 hours between the magnetosphere-ionosphere interaction and the resultant disturbances in the auroral magnetic field for similar reasons and are displayed in Table 1.

In summary, it can be realized from the above study's observations and discussions that the geomagnetic fluctuation is not an instantaneous phenomenon; rather it takes some hourly time or in some cases near about 2 days to build up the interlaying dynamics. Moreover, the proposed coupling function and the threshold value of IMF B_Z, namely, B_{Th}, plays a crucial role in the entire analysis, controlling the area of the cusp width and effectively the amount of input injection, while B_{Th} maintains a direct relationship with the yearly mean total number of sunspots and solar activities for a particular year.

5. Conclusion

Solar wind-magnetosphere coupling is the most significant physical process determining the interlaying dynamical structure of the geomagnetic storm. The energized stream of particles, known as solar wind, interacts with the terrestrial magnetosphere depending on the magnitude and direction of the zth component of the IMF, IMF B_Z. The exact dynamics of solar wind-magnetosphere reconnection process and the subsequent geomagnetic disturbances is a topic of rigorous study for the last decades. In the present paper, we investigated the nature, characteristics, and the effect of this phenomenon on the Earth's magnetosphere based on the concept of self-organized criticality and many-body interactive system. A sandpile-like cellular automata model having a dimension of $n \times n$ and characterized with energy E had been taken as a numerical representation of the terrestrial magnetosphere. The input solar wind energy at any time t can be calculated from the value of real-time ion density and flow speed data. During the reconnection process, an amount of solar wind energy is injected into the magnetosphere through the cusp and alters the energy of the cells of the system. If the total energy of any cell crosses the predetermined threshold value, the excess energy is distributed among its four adjacent neighbors though a small amount of energy is lost during this distribution process. The excess energy reaching the marginal grids dissipates from the system representing the magnetosphere-ionosphere energy transfer process. The model generates two output series. The first one is the series $E_r(t)$, which is an estimation of the total energy trapped in the system at any time t and can be considered as an equivalent to the energy responsible for generation of ring current and the depression of the Earth's horizontal magnetic field from its average value. The second output series $E_a(t)$ is the estimation of excess energy dissipated from the system at any time t and can be taken as a simulated representation of the excess energy released in the ionosphere during magnetosphere-ionosphere interaction which in turn forms the electrojet currents resulting the deviation of auroral magnetic field from its average value.

From our previous study, we came to realize the extreme importance of the solar wind-magnetosphere reconnection regarding the overall geomagnetic disturbances in the Earth and its dependency on the IMF B_Z which motivated us to opt for a deep and involving study of the nature and dynamics of the coupling. In the present paper, we proposed a coupling function to determine the cusp width in terms of IMF B_Z. The cusp width W obeys a hyperbolic tangent function of B_Z, which determines the coupling area depending on the direction and magnitude of B_Z. For extreme northward B_Z, the cusp is almost close whereas it starts to widen out as the magnitude of the northward B_Z reduces below a threshold value B_{Th}. As the B_Z becomes southward, the cusp width further increases proportionally with the increasing magnitude of B_Z and obtains a maximum value for an extremely large southward B_Z. The hyperbolic tangent term in the function numerically varies from 0 to 1 where the value 0 indicates the absolute closing of the cusp and the value 1 indicates absolute opening of the cusp respectively. For the intermediated values, the cusp width is determined according the hyperbolic tangent value of $(-B_Z - B_{Th})$.

To investigate the of the proposed coupling function, the two simulated output series $E_r(t)$ and $E_a(t)$ of the model had been compared with the real-time output of the geomagnetic phenomena, that is, with the real-time *Dst* index series, $E_{Dst}(t + T)$, which is a result of solar wind-magnetosphere interaction and the *AE* index series, $E_{AE}(t + T)$, the result of magnetosphere-ionosphere interaction. To obtain the optimum correlation between the simulated series and the real-time series, in both cases the real-time series had been time shifted by T hours and correlation coefficients had been calculated by varying the value of T. The result shows moderate to high values of correlation coefficients in both the above cases for a specific value of the threshold parameter B_{Th} for each year. Further investigation reveals that the variation of the parameter B_{Th} for the entire solar cycle of the year 1997 to the year 2007 obeys a proportional relationship with the variation of yearly mean total number of sunspots in that solar cycle. This striking outcome indicates direct influence of solar activities on the solar wind-magnetosphere reconnection process. Moreover, for the entire solar cycle, it is observed that a 16- to 43-hr time interval is present between the injection of solar wind energy into the magnetosphere during the magnetic reconnection process, and its subsequent effect on the geomagnetic weather and the depression of terrestrial horizontal magnetic field from its average value. Similarly, in the polar region, the disturbances recorded in the auroral magnetic field at any time t is due to the excess energy released in the ionosphere some 0 to 12 hr before. All these detailed studies and methodical analysis led us to the conclusion that solar wind-magnetosphere energy coupling is controlled by a hyperbolic tangent function of $(-B_Z - B_{Th})$ where the threshold value, B_{Th}, plays the most significant role under the direct influence of solar activities, and the consequent geomagnetic disturbances, far from being an instantaneous phenomenon, possess an intricate underlying structure which needs some hours to nearly a couple of days' time to build up the dynamics and to change the geomagnetic weather in response to the injection of large amount of solar wind energy into the magnetosphere.

The solar wind-magnetosphere coupling is the primary controller of all the geomagnetic fluctuations on Earth. The true nature and actual dynamics of this coupling can reveal important information about all those widely discussed geomagnetic phenomena like geomagnetic storm or auroral disturbances. It is vital to know the exact amount of injected solar wind energy to understand the energy distribution in the magnetosphere along with the magnetosphere-ionosphere energy transfer. A standard coupling function can estimate the total input energy at any time t as well as the nature of the reconnection which enables us to better understand a number of complex mechanisms in the geospace, like the energy distribution process, the transfer of excess energy dissipated into the ionosphere to maintain the equilibrium, the effect of the injected energy on the Earth's magnetic field, and also the time taken for this effect, the occurrence and duration of geomagnetic storm, and many such other fluctuations related to geomagnetic weather. Moreover, the direct relation of the threshold value B_{Th} with the solar activities throws a new light on the overall analysis. The analysis is a first-order trial to investigate the complex natural process for further knowledge, and it did find out some significant points, but simultaneously also indicates the complex and intricate underlying structure possessed by the geomagnetic disturbances. Future work can be directed to acquire detailed knowledge of this structure by developing the model to a higher degree incorporating the other controlling parameters and physical effects in the algorithm.

Acknowledgments
We acknowledge use of NASA/GSFC's Space Physics Data Facility's OMNIWeb (or CDAWeb or ftp) service, OMNI data, and SIDC, RWC Belgium, World Data Centre. Data sets corresponding to Figures and and Table are available as supporting information. We are also thankful to Somnath Mukherjee, Principal of Dinabandhu Andrews College, Kolkata, India, for his cordial support and constant encouragement. Finally, we would like to sincerely thank the anonymous reviewer for his most valuable comments and suggestions to improve the quality of this paper.

References

Akasofu, S. I. (1981). Energy coupling between the solar wind and the magnetosphere. *Space Science Reviews*, *28*, 121. https://doi.org/10.1007/BF00218810

Bak, P., Tang, C., & Wiesenfeld, K. (1987). Self-organized criticality: An explanation of 1/*f* noise. *Physical Review Letters*, *59*, 381–384.

Bak, P., Tang, C., & Wiesenfeld, K. (1988). Self-organized criticality. *Physical Review A*, *38*, 364–372.

Banerjee, A., Bej, A., & Chatterjee, T. N. (2011). On the existence of a long range correlation in the geomagnetic disturbance storm time (*Dst*) index. *Astrophysics and Space Science*, *337*(1), 23–32. https://doi.org/10.1007/s10509-011-0836-1

Banerjee, A., Bej, A., & Chatterjee, T. N. (2015). A cellular automata-based model of Earth's magnetosphere in relation with *Dst* index. *Space Weather*, *13*, 259–270. https://doi.org/10.1002/2014SW001138

Bargatze, L. F., McPherron, R. L., & Baker, D. N. (1986). Solar wind-magnetosphere energy input functions. In Y. Kamide & J. A. Slavin (Eds.), *Solar wind-magnetosphere coupling* (pp. 93–100). Tokyo, Japan: Terrapub/Reidel.

CENTRA Technology, Inc. report (2011). 'Geomagnetic storms,' prepared for the Office of Risk Management and Analysis, United States Department of HomelandSecurity.

Chang, T. S. (1992). Low-dimensional behavior and symmetry breaking of stochastic systems near criticality—Can these effects be observed in space and in the laboratory? *IEEE Transactions of Plasma Science*, *20*(6), 691–694.

Chang, T. S. (1999). Self-organized criticality, multi-fractal spectra, sporadic localized reconnections and intermittent turbulence in the magnetotail. *Physics of Plasmas*, *6*(11), 4137–4145.

Chapman, S. C., Watkins, N. W., Dendy, R. O., Helander, P., & Rowlands, G. (1998). A simple avalanche model as an analogue for magnetospheric activity. *Geophysical Research Letters*, *25*(13), 2397–2400.

Consolini, G. (1997). Sandpile cellular automata and magnetospheric dynamics. In S. Aiello et al. (Eds.), *Conference Proceedings "Cosmic Physics in the Year 2000"* (Vol. 58, pp. 123–126). SIF, Bologna, Italy.
Consolini, G., & Lui, A. T. Y. (1999). Sign-singularity analysis of current disruption. *Geophysical Research Letters*, *26*(12), 1673–1676.
Crooker, N. U., Feynman, J., & Gosling, J. T. (1977). High correlation between long-term averages of solar-wind speed and geomagnetic activity. *Journal of Geophysical Research*, *82*(13), 1933–1937. https://doi.org/10.1029/JA082i013p01933
Crooker, N. U., & Gringauz, K. I. (1993). On the low correlation between long-term averages of solar-wind speed and geomagnetic-activity after 1976. *Journal of Geophysical Research*, *98*(A1), 59–62. https://doi.org/10.1029/92JA01978
Dungey, J. W. (1961). Interplanetary magnetic field and auroral zones. *Physical Review Letters*, *6*(2), 47–48. https://doi.org/10.1103/PhysRevLett.6.47
Finch, I., & Lockwood, M. (2007). Solar wind-magnetosphere coupling functions on timescales of 1 day to 1 year. *Annales de Geophysique*, *25*(2), 495–506.
Gonzalez, W. D. (1990). A unified view of solar-wind magnetosphere coupling functions. *Planetary and Space Science*, *38*(5), 627–632. https://doi.org/10.1016/0032-0633(90)90068-2
Gonzalez, W. D., Tsurutani, B. T., Gonzalez, A. L. C., Smith, E. J., Tang, F., & Akasofu, S.-I. (1989). Solar wind-magnetosphere coupling during intense magnetic storms (1978-1979). *Journal of Geophysical Research*, *94*(A7), 8835–8851. https://doi.org/10.1029/JA094iA07p08835
Hydro-Québec, Understanding electricity (1989).—Hydro-Québec. Retrieved 2010-10-2.
Kan, J. R., & Lee, L. C. (1979). Energy coupling function and solar wind-magnetosphere dynamo. *Geophysical Research Letters*, *6*, 577–580. https://doi.org/10.1029/GL006i007p00577
Kappenman, J. G., Zanetti, L. J., & Radasky, W. A. (1997). *Geomagnetic storms can threaten electric power grid, Earth in space* (Vol. 9, pp. 9–11). Washington, DC: American Geophysical Union.
King, J. H., & Papitashvili, N. E. (2005). Solar wind spatial scales in and comparisons of hourly Wind and ACE plasma and magnetic field data. *Journal of Geophysical Research*, *110*, A02209. https://doi.org/10.1029/2004JA010649
Klimas, A. J., Valdivia, J. A., Vassiliadis, D., Baker, D. N., & Hesse, M. (2000). The role of self-organized criticality in the substorm phenomenon and its relation to localized reconnection in the magnetospheric plasma sheet. *Journal of Geophysical Research*.
Lu, G., Baker, D. N., McPherron, R. L., Farrugia, C. J., Lummerzheim, D., Ruohoniemi, J. M., Rich, F. J., et al. (1998). Global energy deposition during the January 1997 magnetic cloud event. *Journal of Geophysical Research*, *103*(A6), 11,685–11,694. https://doi.org/10.1029/98JA00897
Lu, J. Y., Jing, H., Liu, Z. Q., Kabin, K., & Jiang, Y. (2013). Energy transfer across the magnetopause for northward and southward interplanetary magnetic fields. *Journal of Geophysical Research: Space Physics*, *118*, 2021–2033. https://doi.org/10.1002/jgra.50093
Mawad, R., Kandoul, M., Yousef, S. & Abdel-sattar, W. (2016). Quantizated variability of Earth's magnetopause distance. The 5th International Conference on Modern Trends in Physics Research WSP MTPR-014, Volume 9914, 77-83, 2016 ADS:2016mtpr.conf...77 M.
Murayama, T. (1982). Coupling function between solar-wind parameters and geomagnetic indexes. *Reviews of Geophysics*, *20*(3), 623–629. https://doi.org/10.1029/RG020i003p00623
Newell, P. T., Sotirelis, T., Liou, K., Meng, C.-I., & Rich, F. J. (2007). A nearly universal solar wind-magnetosphere coupling function inferred from 10 magnetospheric state variables. *Journal of Geophysical Research*, *112*, A01206. https://doi.org/10.1029/2006JA012015
NOAA technical memorandum OAR SEC-88 (2003). Halloween space weather storms of 2003, Space Environment Center, Boulder, Colorado, June 2004
Østgaard, N., Germany, G., Stadsnes, J., & Vondrak, R. R. (2002). Energy analysis of substorms based on remote sensing techniques, solar wind measurements, and geomagnetic indices. *Journal of Geophysical Research*, *107*(A9), 1233. https://doi.org/10.1029/2001JA002002
Palmroth, M., Fear, R. C., & Honkonen, I. (2012). Magnetopause energy transfer dependence on the interplanetary magnetic field and the Earth's magnetic dipole axis orientation. *Annales de Geophysique*, *30*(3), 515–526. https://doi.org/10.5194/angeo-30-515-2012
Palmroth, M., Janhunen, P., Pulkkinen, T. I., Aksnes, A., Lu, G., Ostgaard, N., et al. (2005). Assessment of ionospheric joule heating by GUMICS-4 MHD simulation, AMIE, and satellite-based statistics: Towards a synthesis. *Annales de Geophysique*, *23*(6), 2051–2068.
Palmroth, M., Koskinen, H. E. J., Pulkkinen, T. I., Toivanen, P. K., Janhunen, P., Milan, S. E., & Lester, M. (2010). Magnetospheric feedback in solar wind energy transfer. *Journal of Geophysical Research*, *115*, A00I10. https://doi.org/10.1029/2010JA015746
Palmroth, M., Laitinen, T. V., & Pulkkinen, T. I. (2006). Magnetopause energy and mass transfer: Results from a global MHD simulation. *Annales de Geophysique*, *24*(12), 3467–3480.
Palmroth, M., Pulkkinen, T. I., Janhunen, P., & Wu, C. C. (2003). Stormtime energy transfer in global MHD simulation. *Journal of Geophysical Research*, *108*(A1), 1048. https://doi.org/10.1029/2002JA009446
Papadopoulos, K., Goodrich, C., Wiltberger, M., Lopez, R., & Lyon, J. G. (1999). The physics of substorms as revealed by the ISTP. *Physics and Chemistry of the Earth - Part C*, *24*(1–3), 189–202. https://doi.org/10.1016/S1464-1917(98)00028-2
Papitashvili, V. O., Papitashvili, N. E., & King, J. H. (2000). Solar cycle effects in planetary geomagnetic activity: Analysis of 36-year long OMNI dataset. *Geophysical Research Letters*, *27*(17), 2797–2800. https://doi.org/10.1029/2000GL000064
Perreault, P., & Akasofu, S. I. (1978). Study of geomagnetic storms. *Geophysical Journal of the Royal Astronomical Society*, *54*(3), 547–573. https://doi.org/10.1111/j.1365-246X.1978.tb05494.x
Pulkkinen, T. I., Ganushkina, N. Y., Kallio, E. I., Lu, G., Baker, D. N., Turner, N. E., et al. (2002). Energy dissipation during a geomagnetic storm: May 1998. *Advances in Space Research*, *30*(10), 2231–2240. https://doi.org/10.1016/S0273-1177(02)80232-0
Pulkkinen, T. I., Palmroth, M., Janhunen, P., Koskinen, H. E. J., McComas, D. J., & Smith, C. W. (2010). Timing of changes in the solar wind energy input in relation to ionospheric response. *Journal of Geophysical Research*, *115*, A00I09. https://doi.org/10.1029/2010JA015764
Pulkkinen, T. I., Palmroth, M., & Laitinen, T. (2008). Energy as a tracer of magnetospheric processes: GUMICS-4 global MHD results and observations compared. *Journal of Atmospheric and Solar - Terrestrial Physics*, *70*(5), 687–707. https://doi.org/10.1016/j.jastp.2007.10.011
Russell, C. T. (2000). The solar wind interaction with the Earth's magnetosphere: A tutorial. *IEEE Transactions on Plasma Science*, *28*, 1818.
Russell, C. T. (2013). Solar Wind and Interplanetary Magnetic Field: A Tutorial. In P. Song, H. J. Singer, & G. L. Siscoe (Eds.), *Space Weather*. https://doi.org/10.1029/GM125p0073
Scurry, L., & Russell, C. T. (1991). Proxy studies of energy-transfer to the magnetosphere. *Journal of Geophysical Research*, *96*(A6), 9541–9548. https://doi.org/10.1029/91JA00569
Stamper, R., Lockwood, M., Wild, M. N., & Clark, T. D. G. (1999). Solar causes of the long-term increase in geomagnetic activity. *Journal of Geophysical Research*, *104*(A12), 28,325–28,342. https://doi.org/10.1029/1999JA900311
Stern, D. P. (1984). Energetics of the magnetosphere. *Space Science Reviews*, *39*(1–2), 193–213.
Takalo, J., Timonen, J., Klimas, A., Valdivia, J., & Vassiliadis, D. (1999). Nonlinear energy dissipation in a cellular automaton magnetotail field model. *Geophysical Research Letters*, *26*, 1813–1816.

Tanskanen, E., Pulkkinen, T. I., Koskinen, H. E. J., & Slavin, J. A. (2002). Substorm energy budget during low and high solar activity: 1997 and 1999 compared. *Journal of Geophysical Research*, *107*(A6), 1086. https://doi.org/10.1029/2001JA900153

Temerin, M., & Li, X. (2006). *Dst* model for 1995–2002. *Journal of Geophysical Research*, *111*, A04221. https://doi.org/10.1029/2005JA011257

Tenfjord, P., & Ostgaard, N. (2013). Energy transfer and flow in the solar wind-magnetosphere-ionosphere system: A new coupling function. *Journal of Geophysical Research: Space Physics*, *118*, 5659–5672. https://doi.org/10.1002/Jgra.50545

Turner, N. E., Baker, D. N., Pulkkinen, T. I., Roeder, J. L., Fennell, J. F., & Jordanova, V. K. (2001). Energy content in the storm time ring current. *Journal of Geophysical Research*, *106*(A9), 19,149–19,156. https://doi.org/10.1029/2000JA003025

Uritsky V. M. (1996). 1/*f*-like spectra of geomagnetic fluctuations: Expression of self-organized criticality? In Book of abstracts of the International Conference on Problems of Geocosmos, June 17–23, (p. 110). St. Petersburg, Russia.

Uritsky, V. M., & Pudovkin, M. I. (1998a). Fractal dynamics of *AE*-index of geomagnetic activity as a marker of the self-organized criticality in the magnetosphere (in Russian). *Geomagnetizm iAeronomia*, *38*(3), 17–28.

Uritsky, V. M., & Pudovkin, M. I. (1998b). Low frequency 1/*f*-like fluctuations of the *AE*-index as a possible manifestation of self-organized criticality in the magnetosphere. *Annales Geophysicae*, *16*(12), 1580–1588.

Uritsky, V. M., Pudovkin, M. I., & Steen, A. (2001). Geomagnetic substorms as perturbed self-organized critical dynamics of the magnetosphere. *Journal of Atmospheric and Solar-Terrestrial Physics*, *63*(13), 1415–1424. https://doi.org/10.1016/S1364-6826(00)00243-1

Uritsky, V. M., & Semenov, V. S. (2000). A sandpile model for global statistics of reconnection events in the magnetotail. In H. K. Biernat, C. J. Farrugia, & D. F. Vogl (Eds.), *The Solar Wind - Magnetosphere System 3* (pp. 299–308). Osterreichische Akademie der Wissenschaften, Wien.

R.A.M. Van der Linden and the SIDC team (n.d.), online catalogue of the sunspot index, http://sidc.oma.be/html/sunspot.html.

Vasyliunas, V. M., Kan, J. R., Siscoe, G. L., & Akasofu, S. I. (1982). Scaling relations governing magnetospheric energy-transfer. *Planetary and Space Science*, *30*(4), 359–365. https://doi.org/10.1016/0032-0633(82)90041-1

Wang, C., Han, J. P., Li, H., Peng, Z., & Richardson, J. D. (2014). Solar wind-magnetosphere energy coupling function fitting: Results from a global MHD simulation. *Journal of Geophysical Research: Space Physics*, *119*, 6199–6212. https://doi.org/10.1002/2014JA019834

Workshop report, National Research Council of the National Academies (2008). *Severe space weather events—Understanding societal and economic impacts*—. Washington, DC: The National Academies Press.

Wygant, J. R., Torbert, R. B., & Mozer, F. S. (1983). Comparison of S3-3 polar-cap potential drops with the interplanetary magnetic-field and models of magnetopause reconnection. *Journal of Geophysical Research*, *88*(A7), 5727–5735. https://doi.org/10.1029/JA088iA07p05727

Youssef, M., Mahrous, A., Mawad, R., Ghamry, E., Shaltout, M., El-Nawawy, M., & Fahim, A. (2011). The effects of the solar magnetic polarity and the solar wind velocity on *Bz*-component of the interplanetary magnetic field. *Advances in Space Research*, *49*(7), 1198–1202. https://doi.org/10.1016/j.asr.2011.07.023